

<b>DELIVERABLE</b>		<b>5.6.1</b>	
<b>CONTRACT N°</b>	<b>SPC8-GA-2009-233655</b>		
<b>PROJECT N°</b>	<b>FP7-233655</b>		
<b>ACRONYM</b>	<b>CITYHUSH</b>		
<b>TITLE</b>	<b>Acoustically Green Road Vehicles and City Areas</b>		
<b>Work Package</b>	<b>5</b>	<b>Propagation attenuation of road traffic noise</b>	
	<b>5.6</b>	<b>Reduction of low frequency structure borne noise in Brussels</b>	
		<b>Validation report on a solution for low frequency structure borne noise isolation</b>	
<b>Written by</b>	<b>Hamid Masoumi</b>	<b>D2S</b>	
<b>Due submission date</b>	<b>31-12-2012</b>		
<b>Actual submission date</b>	<b>31-12-2012</b>		
<b>Project Co-Ordinator</b>	Acoustic Control	ACL	SE
<b>Partners</b>	Accon	ACC	DE
	Alfa Products & Technologies	APT	BE
	Goodyear	GOOD	LU
	Head Acoustics	HAC	DE
	Royal Institute of Technology	KTH	SE
	NCC Roads	NCC	SE
	Stockholm Environmental & Health Administration	SEP	SE
	Netherlands Organisation for Applied Scientific Research	TNO	NL
	Trafikkontoret Göteborg	TRAF	SE
	TT&E Consultants	TTE	GR
	University of Cambridge	UCAM	UK
	Promotion of Operational Links with Integrated Services	POLIS	BE
	Dynamics, Structures and Systems International	D2S	BE
	Akron NV	AKRON	BE
	<b>Project start date</b>	<b>January 1, 2010</b>	
<b>Duration of the project</b>	<b>36 months</b>		
	<b>Project funded by the European Commission within the Seventh Framework program</b>		
	<b><i>Dissemination Level</i></b>		
PU	Public		✓
PP	Restricted to other programme participants (including the Commission Services)		
RE	Restricted to a group specified by the consortium (including the Commission Services)		
CO	Confidential, only for the members of the consortium (including the Commission Services)		
	<b><i>Nature of Deliverable</i></b>		
R	Report		✓
P	Prototype		
D	Demonstrator		
O	Other		



## TABLE OF CONTENTS

0	Executive summary .....	3
0.1	Objective of the deliverable .....	3
0.2	Description of the work performed since the beginning of the project .....	3
0.3	Main results achieved so far .....	3
0.4	Expected final results .....	3
0.5	Partners involved and their contribution .....	3
0.6	Conclusions .....	3
1	Traffic-induced vibration and structure borne noise .....	4
2	In-situ measurement in the reference site .....	9
3	Numerical modeling of the isolating barrier .....	14
4	Experimental validation by Small-scale test .....	18
5	Measurement setup .....	20
6	Conclusion .....	26
7	References .....	27

## **0 EXECUTIVE SUMMARY**

### **0.1 OBJECTIVE OF THE DELIVERABLE**

Validation of mitigation solutions for low frequency structure borne noise

### **0.2 DESCRIPTION OF THE WORK PERFORMED SINCE THE BEGINNING OF THE PROJECT**

A solution for low frequency structure borne noise has been designed and modelled for a real site in the city.

- A site was selected and traffic-induced vibrations due to passage of a bus over a speed table and a road joint has been measured.
- The numerical tool proposed in the WP4 has been used for modelling and design of the isolating system. The numerical model can account for the road-soil interaction, the wave transmission through the ground, and the structure of the isolating barrier.
- The efficiency of the designed system has been validated by means of an experimental measurement in a scaled test bench.

### **0.3 MAIN RESULTS ACHIEVED SO FAR**

Results of the experimental measurement in the test bench show a reasonable agreement with those predicted by the numerical simulation. This validates the efficiency of the proposed isolating system.

### **0.4 EXPECTED FINAL RESULTS**

The proposed solution for low frequency structure born noise has been validated by means of the experimental measurement in a test bench.

### **0.5 PARTNERS INVOLVED AND THEIR CONTRIBUTION**

D2S was the only partner in this task.

### **0.6 CONCLUSIONS**

In a selected site in the City of Leuven, real traffic-induced vibrations due to passage of a bus over a speed table as well as over a road joint have been measured. Based on the real measured vibration, two types of isolating barrier have been designed and the efficiency of each system has been investigated by both numerical and experimental simulation.

Two types of isolating solution including (1) a single-layer isolating barrier and (2) a multi-layer isolating barrier have been examined. The three-layer barrier consists of two concrete walls and a middle EPS layer. Results of experimental measurements in the scaled test bench show that a three-layer barrier would be more efficient than a one-layer concrete barrier. This confirms results of the numerical modelling presented in WP4.

## 1 TRAFFIC-INDUCED VIBRATION AND STRUCTURE BORNE NOISE

In theory, there is a direct relationship between the vibration of structural elements such as the walls and the floors (slabs) and the noise radiated from the vibrating elements. Therefore, reducing the vibration level at the source level, along the propagation path in the ground, or within the building has a direct influence over the sound pressure in the rooms.

Once the vibration level at the walls or floors has been determined, the acoustic sound power “W” radiated due to the vibration of the walls or floors, can be empirically given in terms of the vibration level of the surface-averaged velocity “ $\bar{v}$ ”, the radiation efficiency ratio “ $\sigma$ ” and the acoustic impedance of the air “ $\rho_0 c_0$ ” [1]:

$$W = \rho_0 c_0 \sigma S \langle \bar{v}^2 \rangle \quad (1)$$

where “S” denotes to the surface of walls or floors.

According to Thompson [1], this equation results in an empirical formulation relating the sound pressure directly to the average velocity on the floor:

$$L_p \approx L_v - 27 \text{ [dB]} \quad (2)$$

where  $L_v$  is the vibration level in dB with a reference of  $1 \times 10^{-9}$  m/s, and  $L_p$  is the sound pressure level in dB with a reference of  $2 \times 10^{-5}$  Pa.

It should be mentioned that in this approximation, the radiation from ceiling and walls has been neglected. However, it can be used for prediction of sound pressure for general buildings.

The problem of traffic-induced vibration and the transmission of this vibration to the building is termed as a dynamic soil-structure interaction problem together with a wave transmission mechanism. To be better comprehensive, the main problem is decomposed into four subproblems (neglecting the vehicle-road interaction) [1, 2]:

- a) The road-ground interaction that refers to how the vehicle load is transferred to the ground nearby the road and it depends on the road type and the soil properties.
- b) The transmissibility of the ground that refers to how the stress wave energy is transmitted through the ground between the road and the building, and it depends on the dynamic properties and the stratification of the soil. Existing public utilities such as the cables, pipes and sewers through the propagation path can significantly influence the transmissibility of the ground.
- c) The ground-foundation interaction that refers to how the ground motion is transferred to the building foundation and it depends mostly on the foundation type, the soil properties and less on the building type
- d) The building response that refers to the dynamic reaction of the building elements (floors or walls) to the incident vibrations at the base level, and it depends on the dimensions and material properties of floors or walls.

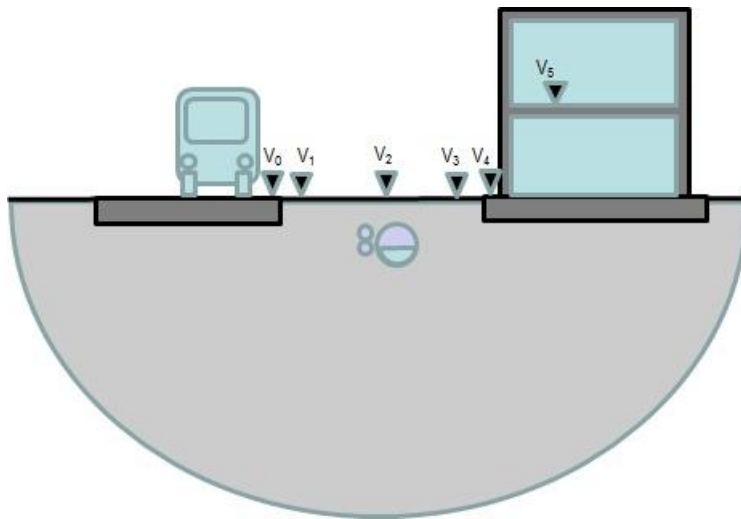


Figure 1

Overview of the problem.

Considering the above expression, the vibration level in the floor can be determined in terms of transfer functions presented in the problem decomposition as follows:

$$L_{v5} = L_{v1} + TF_{GG} + TF_{GF} + TF_{FB} \quad (3)$$

, where  $L_{v1}$  and  $L_{v5}$  are the vibration levels at a location close to the road and at the floor inside the building, respectively. The transfer functions  $TF_{GG}$ ,  $TF_{GF}$  and  $TF_{FB}$  are defined as follows:

$$TF_{GG} = L_{v3} - L_{v1} \quad (4)$$

$$TF_{GF} = L_{v4} - L_{v3} \quad (5)$$

$$TF_{FB} = L_{v5} - L_{v4} \quad (6)$$

The equation (3) shows how any reduction in  $L_{v1}$ ,  $TF_{GG}$ ,  $TF_{GF}$  or  $TF_{FB}$  can result in the reduction in the vibration level  $L_{v5}$  inside the building.

The isolating systems can be classified by their position such that a system installed close to the source is called an active isolation and that installed inside or near to the building (receiver) is a passive isolation, figure 2.

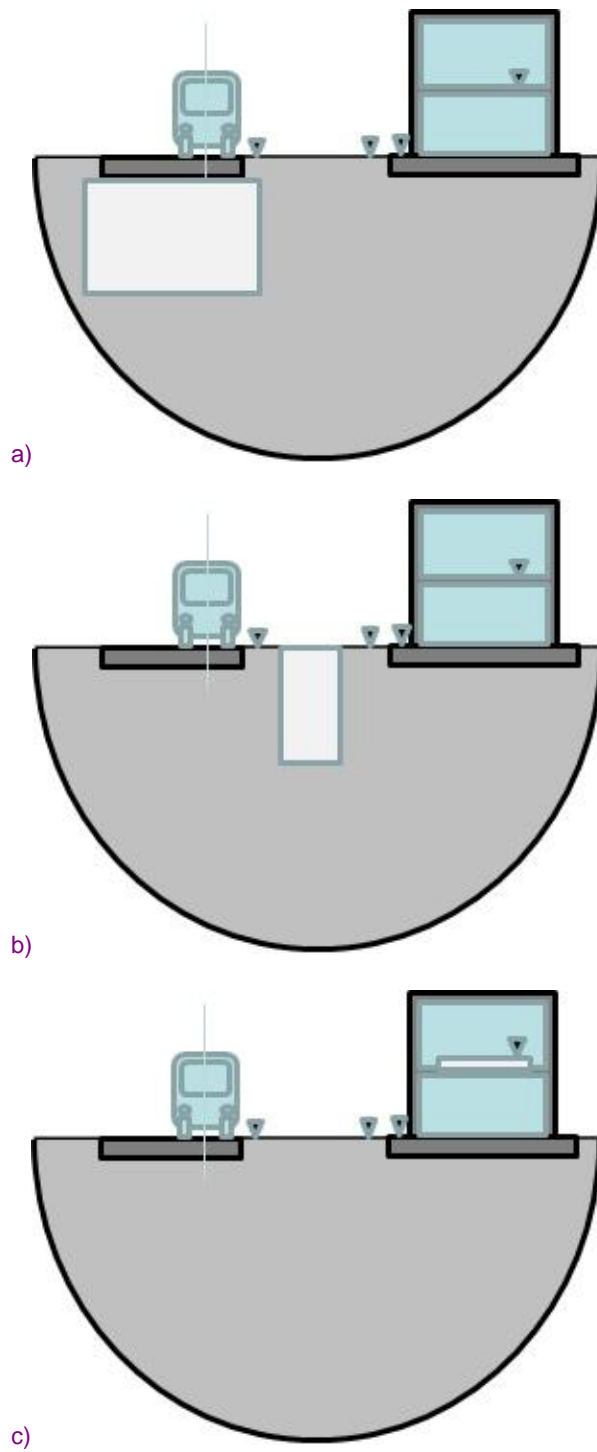


Figure 2 Different isolating solutions: (a) active isolation by improving the soil under the road, (b) the isolating in the propagation path by barriers, and (c) passive isolation by employing an isolating panel in the room

The isolating solutions can be applied in:

- 1) the source level ( $L_{v1}$ ) by improving the ground under and around the road, or by reducing the irregularities and unevenness on the road surface, figure 2a,
- 2) the propagation path ( $TF_{GG}$ ) between the road and the building using isolating barrier or open trenches, figure 2b,
- 3) the building at the foundation level ( $TF_{GF}$ ) using the base isolation systems at the foundation level or in the rooms ( $TF_{FB}$ ) employing the isolating panel, figure 2c.

In the following, as the main objective of this work, the main focus will be on the application of isolating barriers along the propagation path. The problem of traffic-induced vibration mitigation by barriers is termed as a dynamic soil-structure interaction problem together with a wave scattering and wave transmission mechanism.

The characteristics of the induced waves show the existence of three types of the elastic waves. Body waves (shear and compression waves) are most dominant in the soil and propagate in all directions on a spherical wave front. Rayleigh waves however propagate radially on a cylindrical wave front along the surface.

Most of the vibration energy affecting the buildings and structures in the far field is carried by Rayleigh waves that propagate in a zone close to the ground surface. However, in the near field, the ground motion is mostly dominated by the shear or the compressional waves.

The energy of induced waves can be reduced by installing a wave barrier system against the wave propagating direction. This results in the reflection, damping and scattering of the incoming waves.

In addition, traffic-induced vibrations are mainly due to the interaction between the vehicle (wheels) and the road surface. The dynamic axle loads are determined by the vehicle dynamics, the road unevenness and the road flexibility [3,4, 5]. According to Pyl et al. (2004) [4], the axle's peak acceleration increases almost linearly with increasing vehicle speeds. However, this trend is not observed for the rear axle. Further, the dominant frequency of generated ground vibrations is mainly determined by the axle hop modes of the vehicle as well as the type of the road unevenness and is not influenced by the vehicle speed.

Figure 3 shows a procedure that is proposed for designing of an isolating barrier as well as the validation of its efficiency by an experimental small-scale test.

Since a full-scale test is expensive, a small-scale test has been performed to validate the efficiency of the designed barrier.

First, a reference site is selected and the vibration level at different points between the road and the building as well as the ground transmissibility are measured due to road traffic. The vibrations may be generated due to passage of a bus over a speed table or a road joint. The geometry of the road unevenness affects the frequency content and the amplitude of induced ground vibrations.

Then, using a numerical modelling, the isolating barrier is designed. The main parameters such as the distance from the road  $R_b$ , the height  $H_b$  and the width of the barrier  $W_b$  will be selected and the efficiency of barrier is determined by means of a numerical simulation using a coupled BEM-FEM model.

Finally, results of the numerical modelling (e.g. the efficiency of the barrier) are validated by means of an experimental small-scale test.

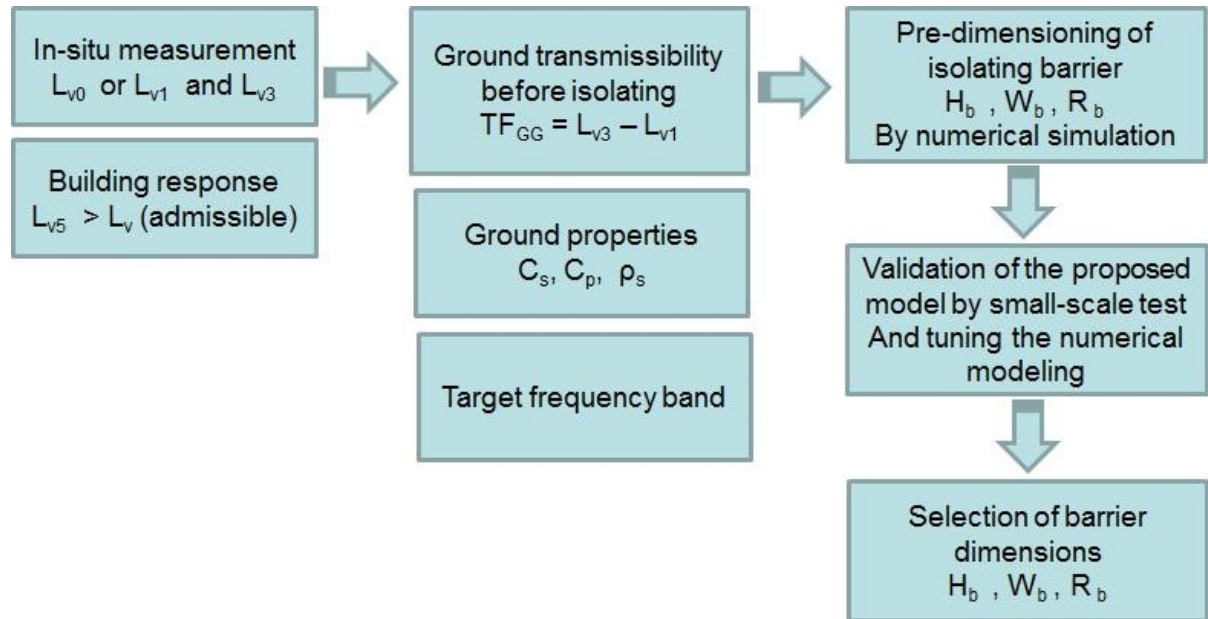


Figure 3

Proposed procedure for design of the isolating barrier

## 2 IN-SITU MEASUREMENT IN THE REFERENCE SITE

The ground vibrations due to passage of some buses are measured in a site in an urban area. The site is located at Koning Albert street in Leuven (in Belgium). Two locations are selected: location (A) along a speed table in the street and location (B) along a road joint, figure 4.

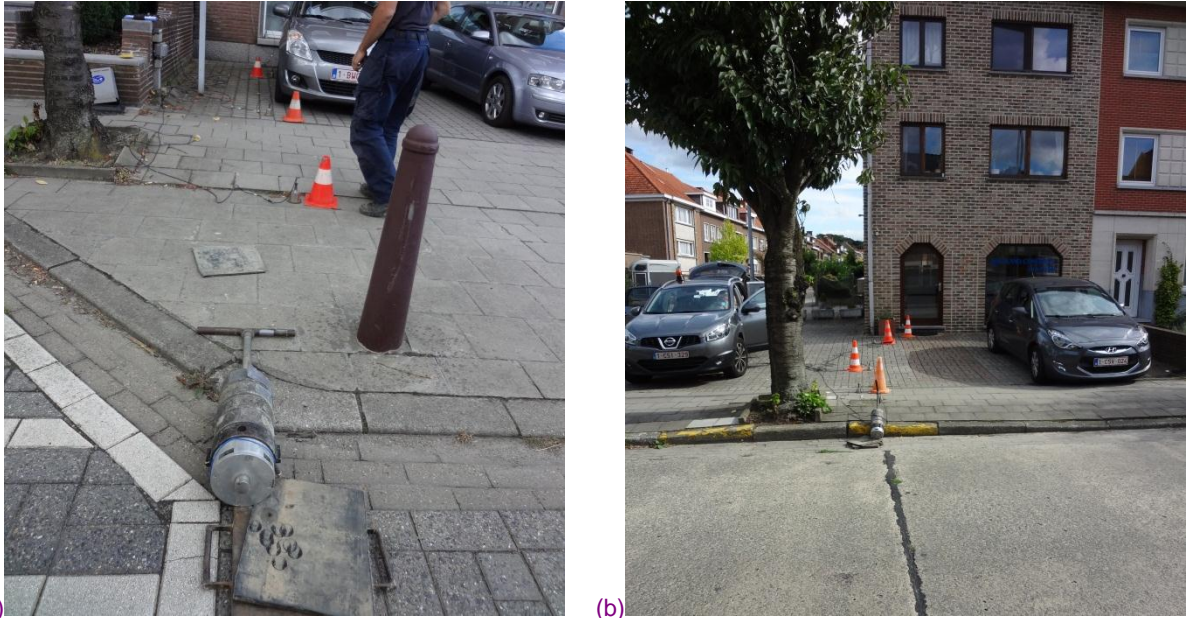


Figure 4 (a) In-situ measurement in (a) the location A along a speed table and (b) the location B along a road joint

According to the geological map of the region, the site is situated over a Brussels formation and the ground consists of the grey fine sand, lime, and lime sandstone from surface layer to the depth, respectively, figure 5.

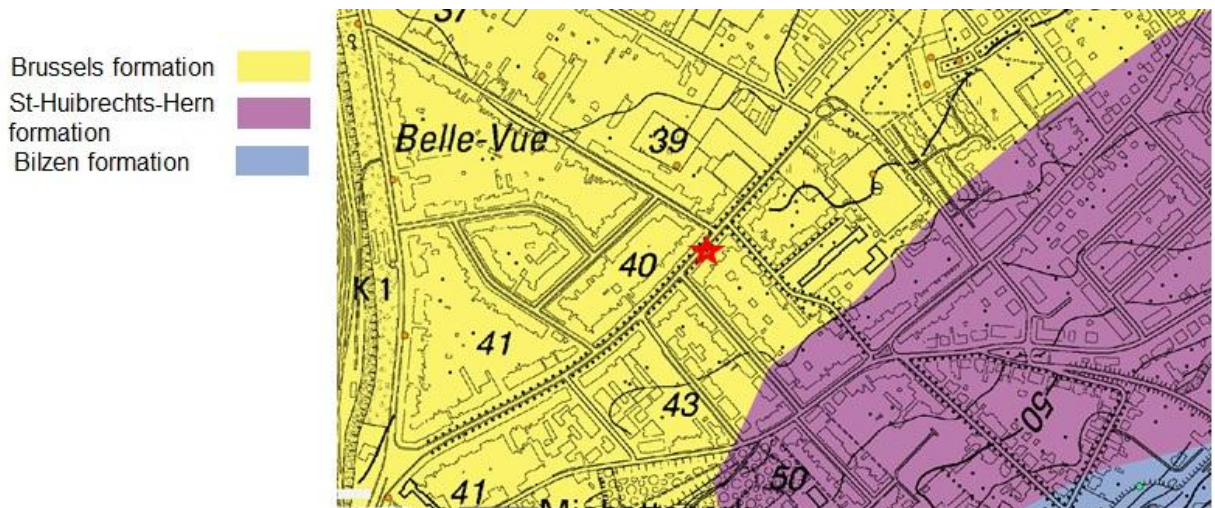


Figure 5 Geological map of the selected site, Kessel-lo (Leuven)

The cone penetration test at the locations near to the test site shows a soft layer with the cone resistance  $q_c < 2$  Mpa from 0 to 2.0 m and a medium stiff layer with  $2 \text{ Mpa} < q_c < 8$  Mpa from 2.0 to 5.0 m that is resting on a stiff soil with  $q_c > 15$  Mpa.

The ground vibrations are measured along two measurement lines perpendicular to the road direction. At each location, the measurement setup consists of 4 1v/g accelerometers ( $V_1$ ,  $V_2$ ,  $V_3$ , and  $V_4$ ) such that three of them ( $V_1$ ,  $V_2$ , and  $V_3$ ) are placed on the ground surface between the road and the nearby building, and one accelerometer ( $V_4$ ) is placed in the foundation level of the building.

Figure 6 shows the ground vibrations measured at the location A and B. Results of a single event are presented in terms of the autopower spectrum in third octave frequency bands.

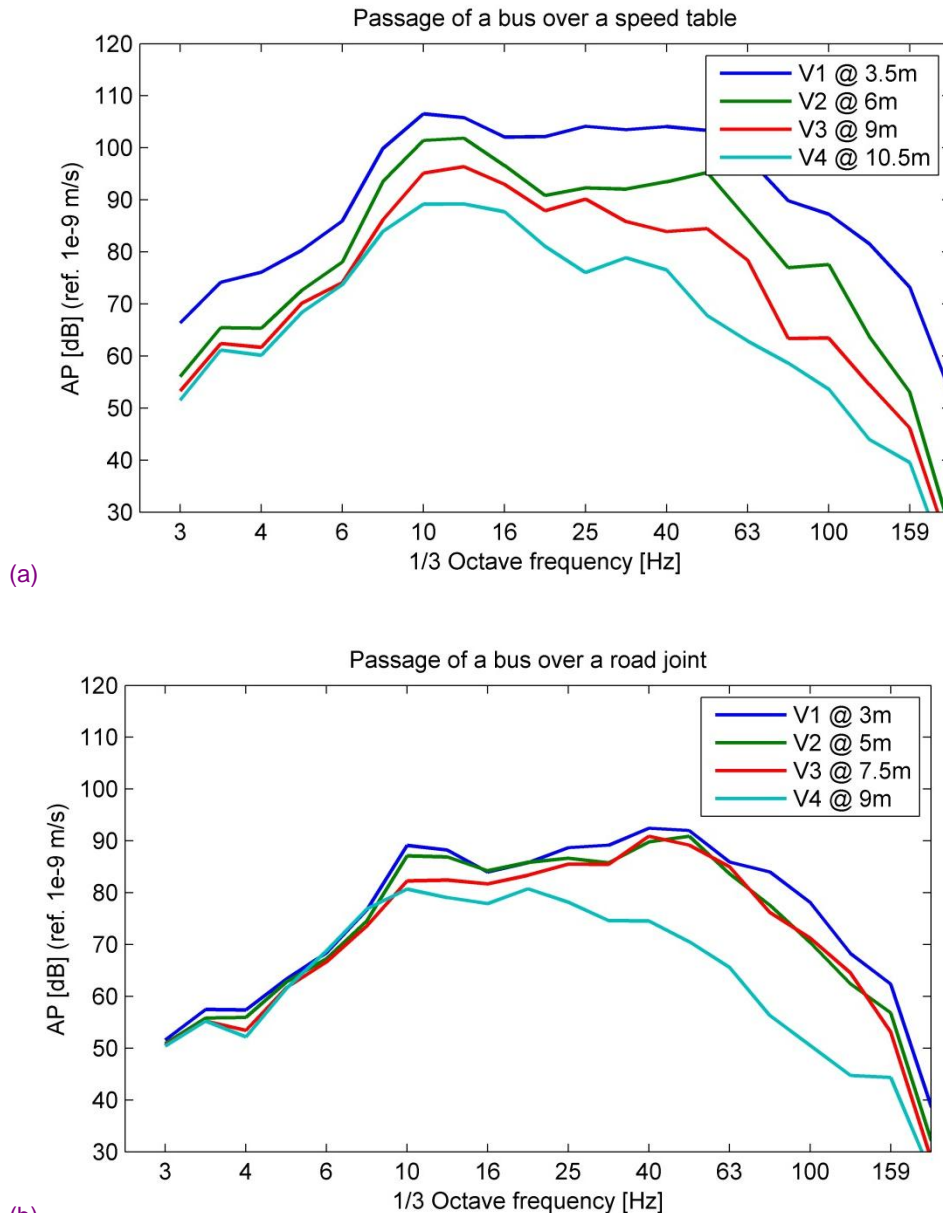
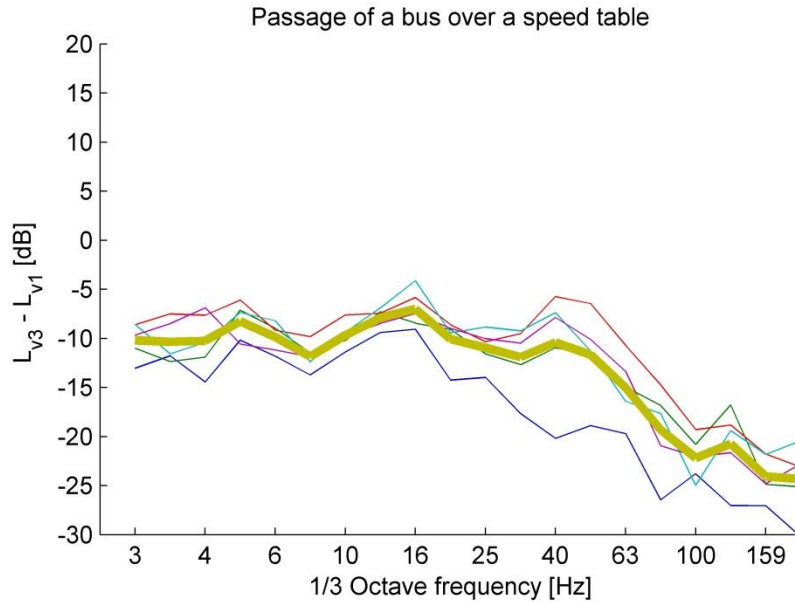


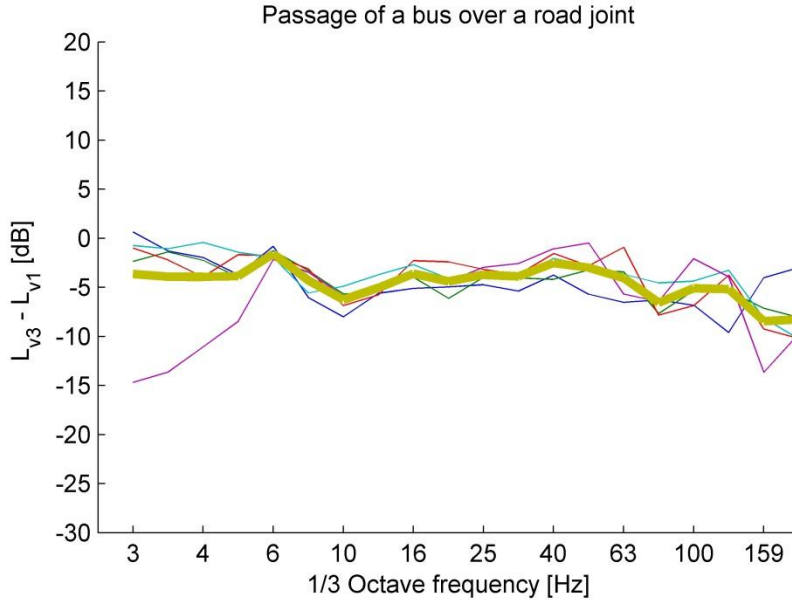
Figure 6 (b) Autopower spectrum of the ground vibrations (a) due to passage of the bus over the speed table and (b) due to the passage of the bus over the joint

Results show that the passage of the bus over the speed table generates higher vibration compared to that measured due to the passage of the bus over the joint.

Figure 7 shows the transmissibility function  $TF_{GG}$  (the transfer function between points  $V_3$  and  $V_1$ ) measured due to several passages. Results in the location A show higher vibration attenuation compared to those obtained in the location B.



(a)

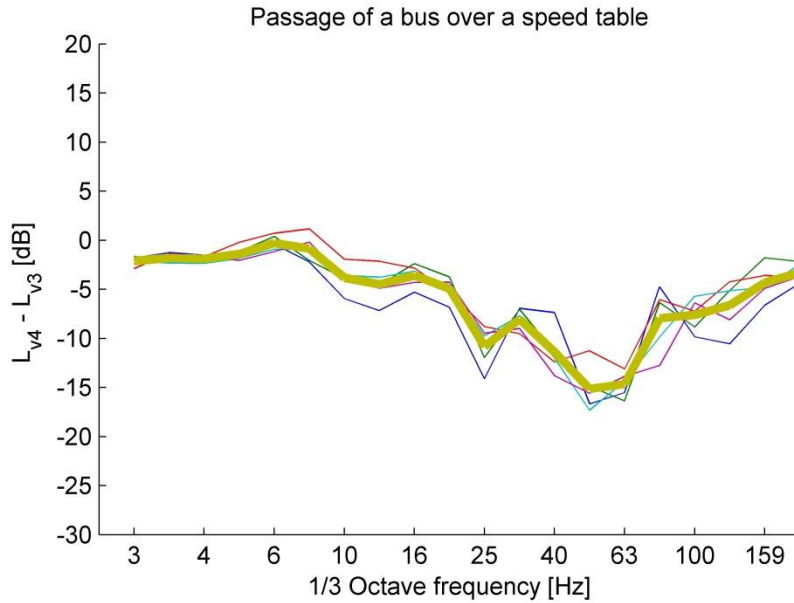


(b)

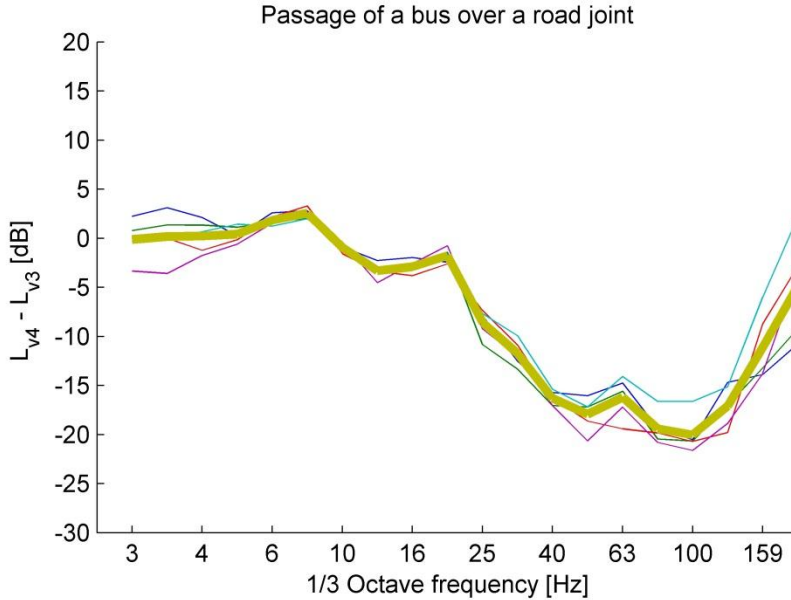
Figure 7 Transmissibility function of the ground measured in (a) the location A, and (b) in the location B

Different vibration attenuation patterns observed between two locations can be explained by the fact that different ground conditions in each location such as the inhomogeneity of soil and the presence of public utilities and sewers within the ground, can significantly affect the wave transmissibility of the soil medium, especially at higher frequencies.

Considering the vibrations measured at points  $V_3$  and  $V_4$ , the ground-foundation transfer function is calculated by means of equation (5). Figure 8 shows the ground-foundation transfer function in both location A and B.



(a)



(b)

Figure 8 Ground-foundation transfer function measured in (a) the location A, and (b) in the location B

Results show a significant vibration attenuation at frequencies higher than 16 Hz in both locations. In addition, higher attenuation is observed at location A compared to that obtained in the location B. This is due to the different foundation or soil conditions in the measurement locations. As mentioned before, the foundation-ground transfer function depends on the foundation type and the ground properties.

Since different buildings are placed at the reference site and there was no access to interior of all buildings, an approximate estimation has been considered for the foundation-building transfer function. According to Pyl et al. [4], the floor to foundation resonance shows an amplification from 10 to 20 dB at a frequency range from 10 to 20 Hz depending on the floor dimensions and its material properties.

According to the results of the measurement site, the vibration level in floor ( $V_f$ ) and consequently the sound pressure in the room are conservatively determined by means of equations (2) and (3).

In the next step, to mitigate the structure borne noise in the building, an isolating barrier system is designed.

### 3 NUMERICAL MODELING OF THE ISOLATING BARRIER

In designing an efficient isolating barrier, the main objective would be to shift the frequency of the induced waves into higher ones (smaller wavelength) as well as reducing the vibration amplitude by the impedance jump between the layers.

In practice, the construction of a very deep barrier becomes more difficult and consequently, more expensive with increasing depth. According to results of WP4, a three-layer barrier with a middle soft layer would be more efficient than a deeper one-layer barrier. Therefore, two types of barrier are proposed and the efficiency of each barrier is numerically computed.

A 2.5-dimensional coupled FE-BE modelling is used for computation of the dynamic interaction between the soil and the structure (the road and the barrier). In 2.5-dimensional modelling, a longitudinally invariant geometry of the structure (the road or the barrier) is assumed, [6].

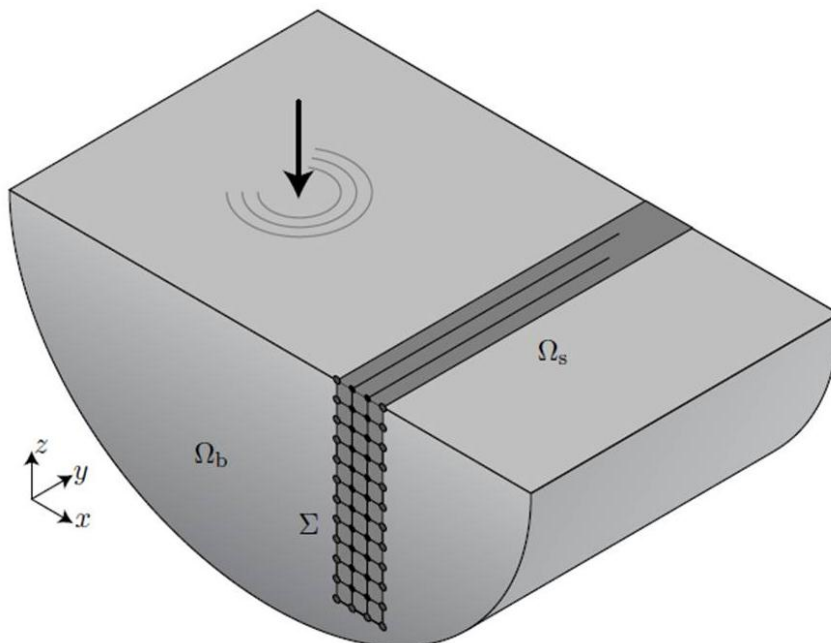


Figure 9

Overview of 2.5D modelling, after François et al. [8]

In this approach, the problem is transformed into a sequence of two-dimensional (xz-plane) models in terms of the wavenumber in the track direction (y-direction). For each discrete wavenumber in y-direction, the finite cross section of the structure is modelled using conventional plane strain FEM (two-dimensional FEM) and the surrounding soil with plane strain BEM, figure 9. The coupled FE-BE model is solved for each wavenumber value. The response, therefore, at different y-direction is calculated by means of an inverse Fourier Transformation. This method is termed as the wavenumber FE-BE method or 2.5-dimensional FE-BE modelling, [6, 7].

The 2.5D green's functions of the soil, computed by the direct stiffness method, are used in a boundary element method formulation. The direct stiffness method has been implemented in the MATLAB toolbox EDT for elastodynamic wave propagation in layered media [8]. This avoids meshing of the free surface and the layer interfaces with boundary elements and effectively reduces the computational efforts and storage requirements.

In this methodology, 2.5D FEM is used to model the structure (the road and the barrier) and the soil impedance as well as the free field vibrations are computed by means of 2.5D BEM. This methodology has been already examined for different applications such as railway tracks, roads, tunnels, dams, trenches, and pipelines by François et al. [6].

The barrier is a concrete wall that has a height  $H_b$ , a thickness  $W_b$  and is located at distance  $R_b$  from the vibration source: the road, figure 10. The three-layer barrier consists of two concrete walls and the space between the walls is filled by the extruded-polystyrene (EPS). The dimensions of the proposed models are presented in table 1.

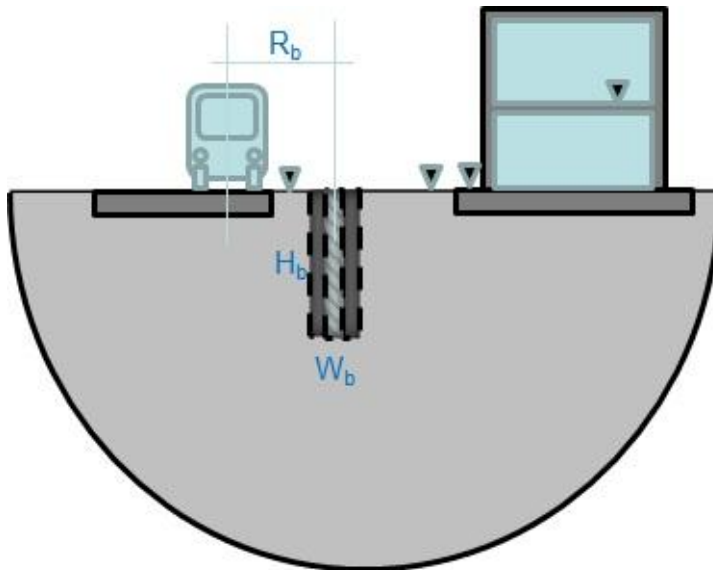


Figure 10

Overview of the isolating system

Concrete barrier	$W_p = 0.60 \text{ m}$	$H_p = 9.0 \text{ m}$	$R_p = 2.25 \text{ m}$
Concrete-EPS-Concrete barrier	$W_p = 3 \times 0.6 \text{ m}$	$H_p = 6.0 \text{ m}$	$R_p = 2.25 \text{ m}$

Table 1 Dimension of proposed isolating barrier

The soil medium is a homogeneous half space with Young's modulus  $E_s = 108 \text{ Mpa}$ , a Poisson's ratio  $\nu_s = 0.33$ , a material density  $\rho_s = 1,800 \text{ kg/m}^3$ , and a material damping  $\beta_s = 2.5\%$ . The shear and compression wave velocities of the soil are 150 m/s and 300 m/s, respectively. According to the material properties, the impedance ratio concrete to soil and concrete to EPS are 15 and 3200, respectively.

The concrete has a Young's modulus  $E_c = 30,000 \text{ Mpa}$  a Poisson's ratio  $\nu_s = 0.25$ , and a material density  $\rho_c = 2,500 \text{ kg/m}^3$ . The extruded-polystyrene has a Young's modulus  $E_e = 2 \text{ Mpa}$ , a Poisson's ratio  $\nu_e = 0.15$ , and a material density  $\rho_e = 12 \text{ kg/m}^3$ , [9].

A frequency analysis within a range of frequency from 5 to 60 Hz has been done by applying a unit vertical force on the road. The element size in BE and FE models is selected sufficiently small respect to the minimum wavelength  $\lambda_{\min} = \min(C_s) / f_{\max}$ , where  $\min(C_s)$  denotes to minimum shear wave velocity of the materials used in the model, and  $f_{\max} = 60 \text{ Hz}$  is the maximum frequency of the interest. A mesh sampling of at least 8 elements over one wavelength is considered.

Three calculations are done and free field vibrations are computed for a) the reference case where no barrier exists, b) concrete barrier, and c) the concrete-EPS-concrete barrier.

Figure 11 shows the mobility function on the soil surface at 16 m from the road centre. The results show that the three-layer barrier very well decreases the vibration amplitude for frequencies higher than 10 Hz.

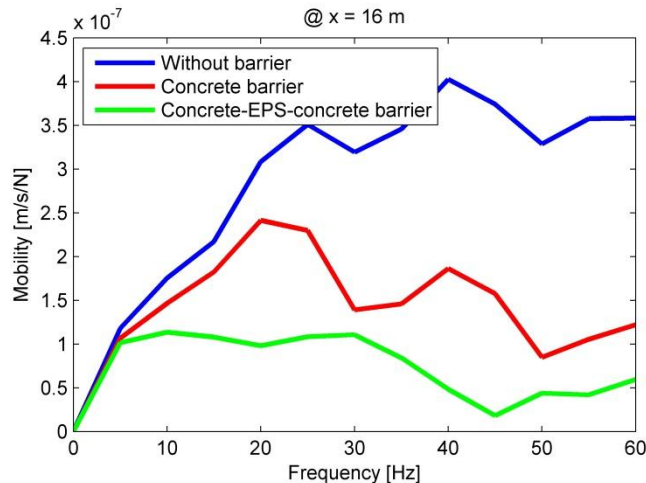


Figure 11

Mobility function on the soil surface at 16 m from the source, computed for different barrier configurations

The efficiency of the isolating system can be evaluated by the insertion loss factor  $IL$  in dB as follows:

$$IL_{[dB]} = 20 \times \log_{10} \left( \frac{\hat{u}_{isolated}}{\hat{u}_{non-isolated}} \right) \quad (7)$$

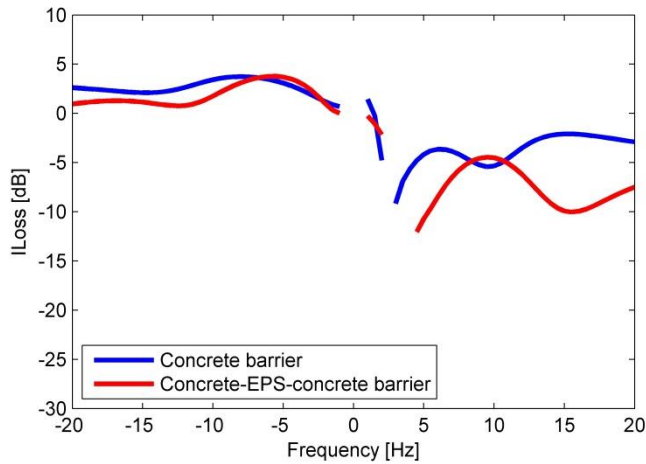
where  $\hat{u}(\omega)$  is the vibration amplitude in the frequency domain.

As the insertion loss changes with the distance from the barrier, this factor can be presented as an average value for a set of points in an area or along a line behind the barrier. Therefore, the average insertion loss factor  $\overline{IL}$  can be calculated as follows:

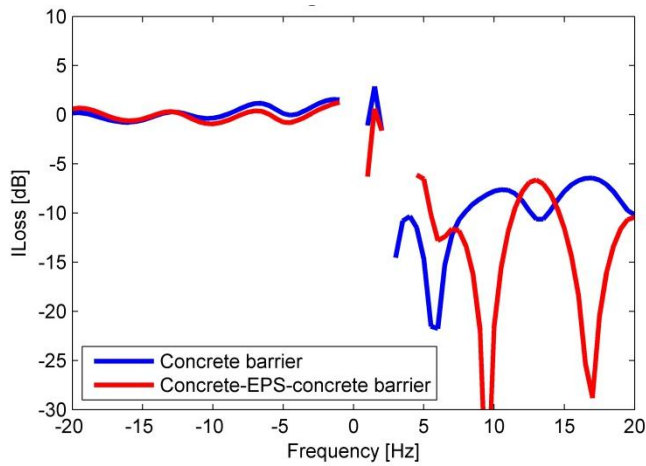
$$\overline{IL}_{[dB]} = \frac{1}{x_2 - x_1} \int_{x_1}^{x_2} IL_{[dB]}(x) dx \quad (8)$$

where  $x$  denotes to the distance of the receivers from the barrier.

Figure 12 shows variation of the insertion loss versus the distance from the source at 20 and 40 Hz. The results display higher attenuation when a three-layer barrier is employed. In addition, at 40 Hz, very high attenuation is obtained by all barriers.



(a)



(b)

Figure 12 Comparison of the insertion loss versus distance from the source at (a) 20 and (b) 40 Hz, computed for different barrier configurations

Figure 13 shows the insertion loss factor versus the frequency computed by the equation (6) for both barrier configurations in the ground surface at 16 m from the road.

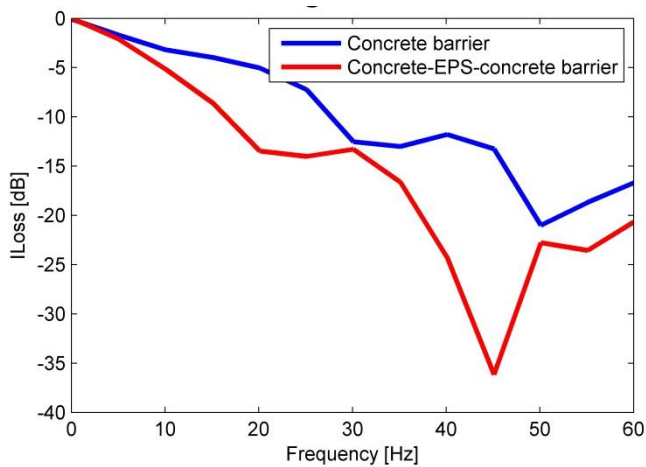


Figure 13 Comparison of the insertion loss versus excitation frequency in a point located at 16 m from the road, computed for different barrier configurations

## 4 EXPERIMENTAL VALIDATION BY SMALL-SCALE TEST

To validate the results of the numerical prediction model, a small-scale test is performed. The test bench consists of (1) a soil container, (3) an isolating screen (a barrier), and (3) soil (a clean fine sand), figure 14.

Some difficulties for realizing the boundary conditions in the test bench are resolved by selecting an appropriate scaling factor as well as a relevant dimension for the soil container. On the other hand, considering the soil container's size and the dominant frequency of the induced vibrations, a scaling factor must be chosen [10].

The selected soil is the Mol silica sand, type M32 from SIBELCO, with an average grain size (D50) of 0.26 mm and a dry density of 1700 kg/m<sup>3</sup>. The sand is very well sieved, washed and then dried and classified.

The pluviation method or sand raining is used to fill the container. This method provides a uniform and homogeneous sand specimen in the test bench. More details on soil treatment have been presented in the deliverable of WP4.

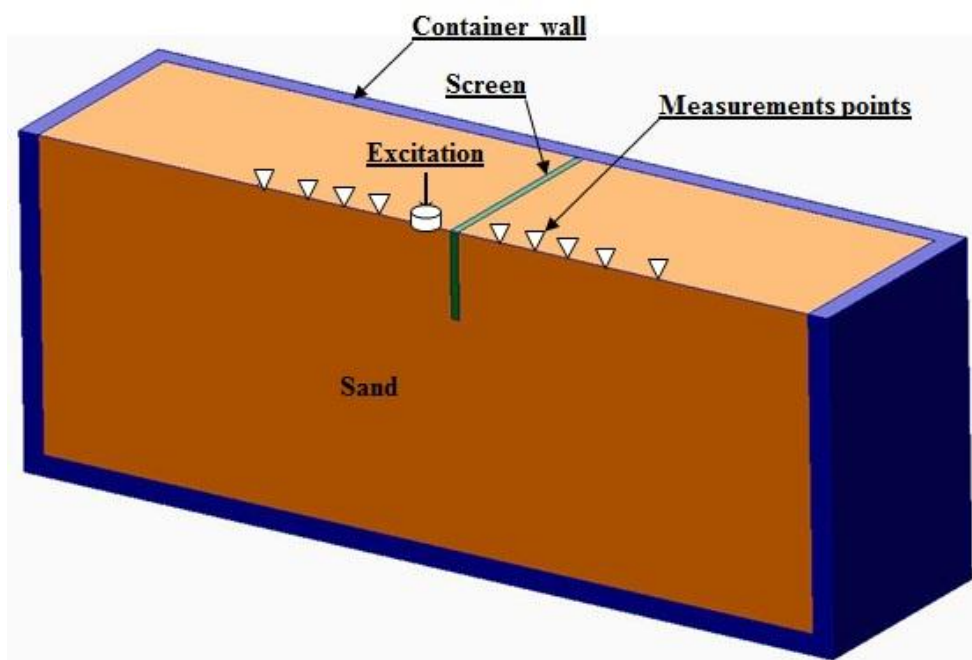


Figure 14

Overview of the test bench

Since traffic induced vibrations are dominant in a frequency range from 10 to 50 Hz, the isolating system must be effective around this frequency range. Therefore, a reasonable scaling factor and consequently an effective isolating barrier dimension in the frequency range of interest must be selected.

A geometric scaling factor  $N = 15$  is selected. Table 2 shows the dimensions of the small-scale model associated to the selected scaling factor  $N = 15$ .

According to the frequency range of interest from 10 to 50 Hz in the prototype (full scale), the experiment measurement in the test bench must be performed within the frequency range from 150 to

750 Hz. Table 2 shows the dimensions of the scaled model using the scaling factor  $N = 15$ .

	Frequency range [Hz]	Concrete barrier			Concrete-EPS-Concrete barrier		
		$W_b$	$H_b$	$R_b$	$W_b$	$H_b$	$R_b$
Small-scale $N = 15$	100 - 900	0.04 m	0.60 m	0.15 m	3*0.04 m	0.40 m	0.15 m
Full-scale	6.7 – 60	0.60 m	9.0 m	2.25 m	3*0.60 m	6.0 m	2.25 m

Table 2 Dimensions of scaled model in the test bench

## 5 MEASUREMENT SETUP

The measurement configuration consists of a small foundation posed on the soil surface where the dynamic force is applied and accelerometers mounted at the measurement points. The barrier is installed at a specific distance on one side from the foundation. The small foundation is excited at the frequency band of interest and the free field vibrations are measured at the different points.

A total of 10 accelerometers 100 mv/g are located on the soil surface symmetrically on both sides of the foundation. This configuration enables us to simultaneously measure with the same soil and excitation condition, the non-isolated response (on the side without the barrier) and the isolated response (on the side where the barrier is installed), figure 15. The measurement points  $V_1$  to  $V_5$  represent the ground responses in the non-isolated side and the measurement points  $V_7$  to  $V_{10}$  represent the ground responses in the isolated side. The measurement point  $V_6$  is located on the barrier and represent the vertical response of the barrier.

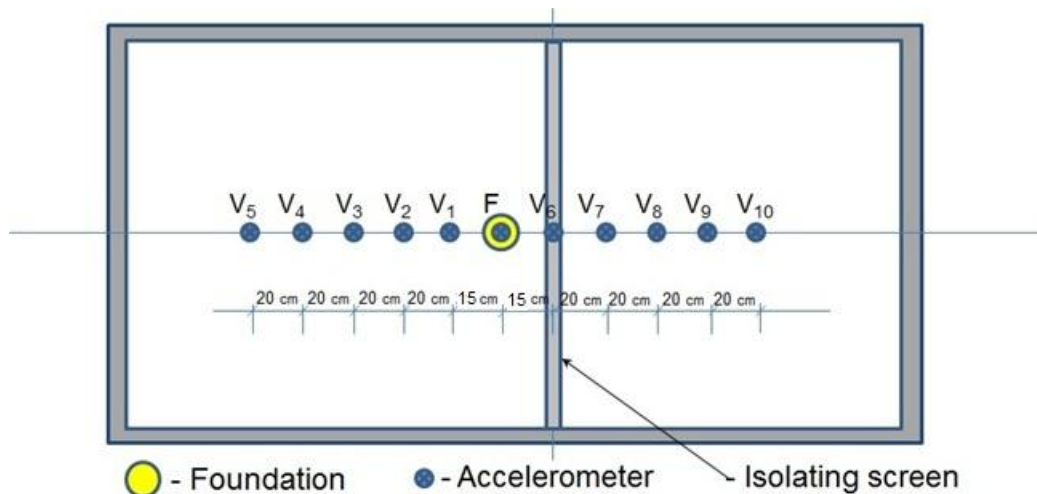


Figure 15

Overview of the measurement setup

A 24 bit National Instrument data-acquisition system, coupled to a portable PC is used for A/D conversion, figure 14. The A/D conversion is performed at a sampling rate of 4000 Hz that results in a Nyquist frequency of 2000 Hz.

A shaker device is used for the excitation generation. The shaker is installed over a small foundation. The type, the amplitude and the frequency content of the excitation can be controlled by means of a wave generator software that feeds into a power amplifier, figure 16. A random vibration was applied at different frequency range from 100 to 900 Hz.

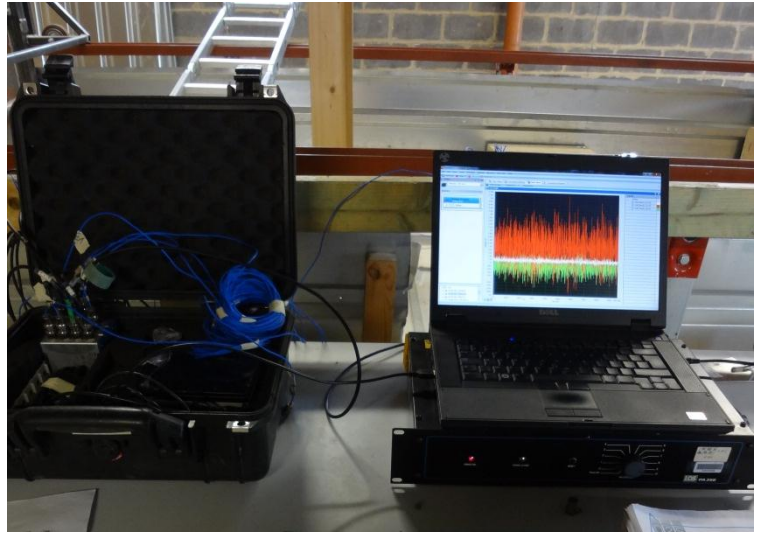


Figure 16

Shaker device and acquisition system

Table 3 shows the frequency ranges that have been applied for the measurements. Based on five frequency ranges, four separate measurements were performed. In fact, a random excitation but at different range of frequencies is applied. To obtain a reasonable coherency, the excitations were applied for a period of at least 3 minutes.

Frequency range [Hz]	
Small-scale test N=15	Full-scale test
100-300	6.7 - 20
300-500	20 - 33.3
500-700	33.3 - 46.7
700-900	46.7 - 60

Table 3 Frequency ranges in the full scale and the small-scale test

The free field response at the non-isolated side is considered as the reference vibration. To obtain the isolation efficiency of the isolating barrier, the results of this reference vibration are compared with those measured at the isolated side.

Figures 17 and 18 show the configuration of the measurements for two tested barriers. The efficiency of two barriers were evaluated in the same soil conditions and the measurement configuration.



Figure 17

Measurement configuration for the concrete barrier test

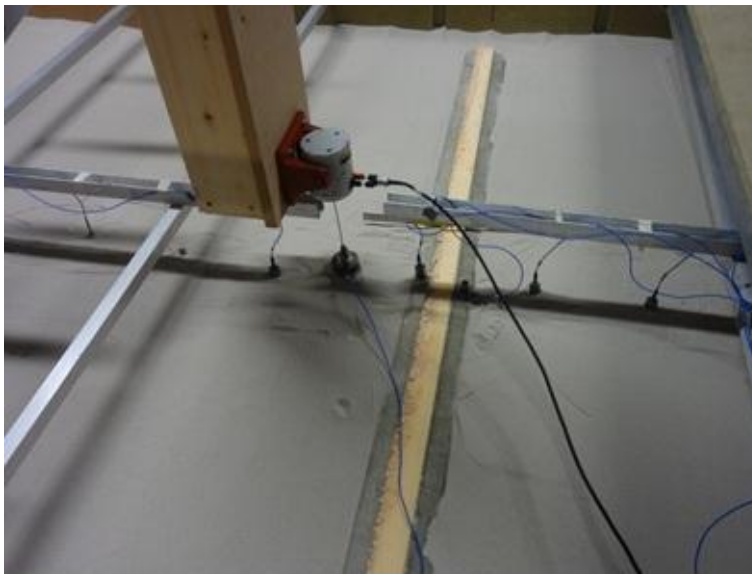


Figure 18

Measurement configuration for the concrete-EPS-concrete barrier test

The insertion loss was computed using the peak particle velocity (PPV) obtained at each measurement points.

$$IL_{[dB]} = 20 \times \log_{10} \left( \frac{PPV_{isolated}}{PPV_{non-isolated}} \right) \quad (9)$$

where the peak particle velocity (PPV) is defined as the maximum value of the impulse response function (IRF) at each measurement points.

The frequency range as well as the distance from the source are presented in the real scale.

Figures 19 and 20 show the variation of the insertion loss versus the distance for both barriers. Results of the experimental test bench are compared with those computed by the numerical modelling. A remarkable agreement between the experimental and numerical simulation has been observed for the concrete barrier case. The numerical modelling display a conservative efficiency for three-layer barrier the points close to the barrier. However, a reasonable agreement has been obtained at the points from 8 to 14.

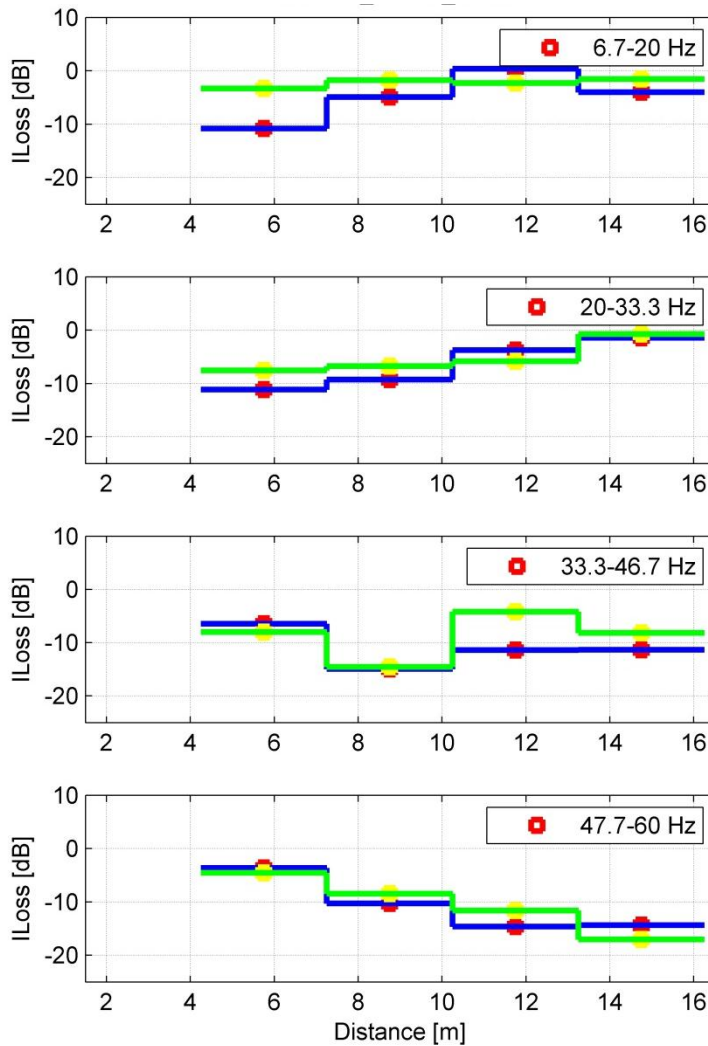


Figure 19

Insertion loss versus distance from the source at different frequency ranges - Results of the concrete barrier in the small-scale test (blue line) are compared with those of the numerical modelling (green line)

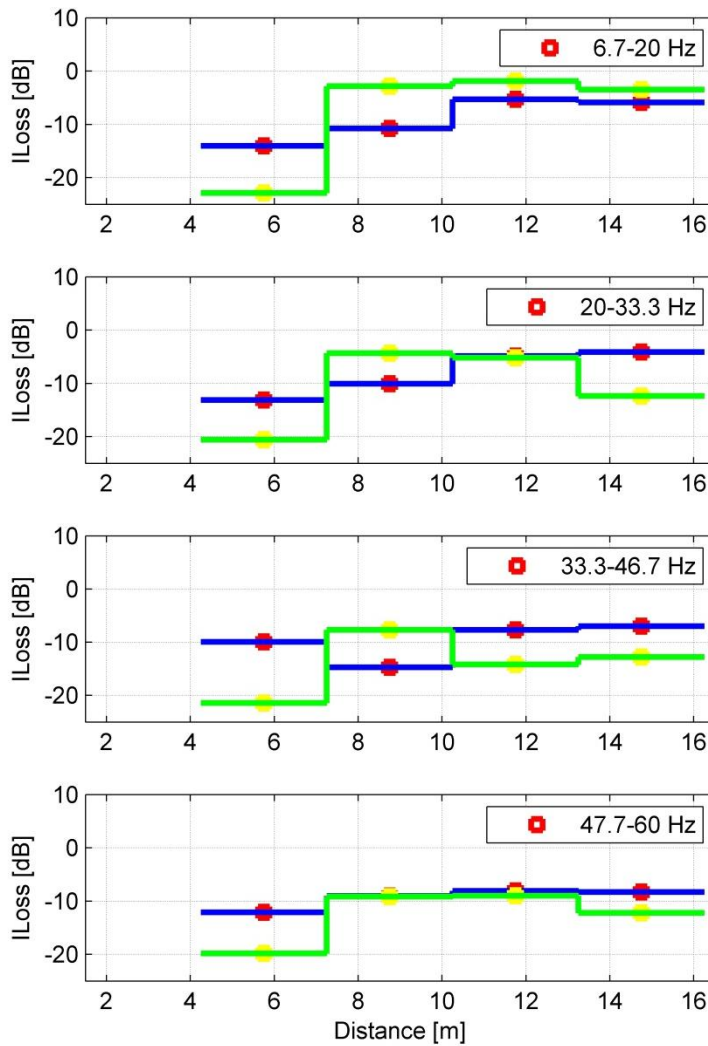


Figure 20

Insertion loss versus distance from the source at different frequency ranges - Results of the concrete-EPS-concrete barrier in the small-scale test (blue line) are compared with those of the numerical modelling (green line)

Using the equation (8), an average insertion loss is calculated for each barrier over all measurement points. Figures 21 and 22 show the average insertion loss for both barriers. Results of the experimental test bench are compared with those computed by the numerical modelling. The frequency ranges are presented in the real scale.

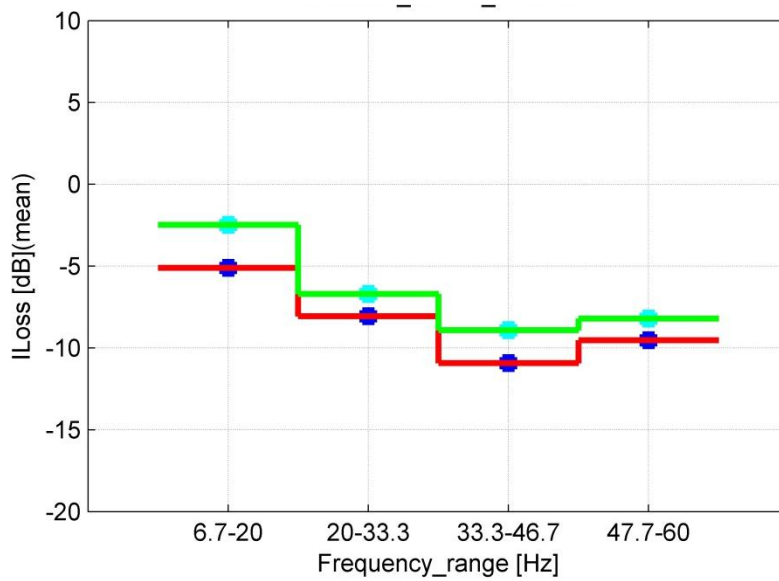


Figure 20

Average insertion loss computed for different frequency ranges - Results of the concrete barrier in the small-scale test (red line) are compared with those of the numerical modelling (green line)

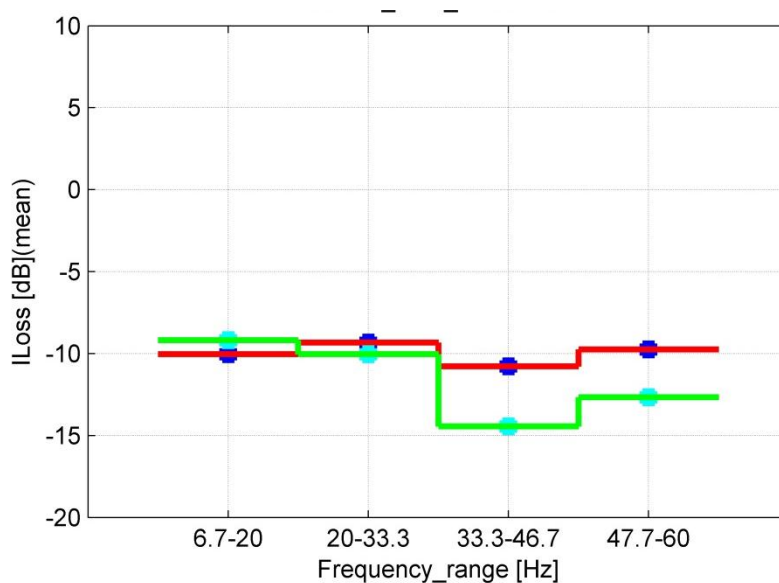


Figure 21

Average insertion loss computed for different frequency ranges - Results of the concrete-EPS-concrete barrier in the small-scale test (red line) are compared with those of the numerical modelling (green line)

Results of the experimental measurements show very good agreement with those predicted by the numerical modelling. A reasonable discrepancy of maximum 3 dB for the concrete barrier and 5 dB for concrete-EPS-concrete barrier is observed.

Furthermore, results of both the numerical and experimental simulation confirm that the proposed isolating barrier consisting of three layers (concrete, EPS and concrete) would be an efficient mitigation solution for the traffic-induced vibrations.

## 6 CONCLUSION

Two types of isolating solution (1) a concrete barrier and (2) a concrete-EPS-concrete barrier have been designed. Results of experimental measurements in the scaled test bench show that a three-layer barrier would be more efficient than a one-layer barrier. This confirms results of the numerical modelling presented in WP4.

To have an estimation on the noise reduction, the level of the insertion loss at a point close to the building (at around 10 m from the road) should be considered. Then, the level of noise reduction can be determined using the equation (2). The following table shows a resume of the noise reduction inside the building using different barrier configurations.

Frequency range [Hz]	Concrete barrier $H_b = 6$ [m]		Concrete-EPS-concrete barrier $H_b = 6$ [m]	
	$H_b/\lambda$ [-]	IL [dB]	$H_b/\lambda$ [-]	IL [dB]
6.7 - 20	0.8	2	0.53	7
20 - 33.3	1.6	7	1.1	9
33.6 - 46.7	2.4	11	1.6	12
46.7 - 60	3.2	12	2.1	10

Table 4 Noise reduction inside the building versus real frequency range

To obtain higher efficiency, deeper barriers with higher depth ratio  $H_b/\lambda$  must be used. For instance, using a concrete-EPS-concrete barrier of 8 m (with  $H_b/\lambda = 1.4$ ) or a concrete barrier of 13 m ( $H_b/\lambda = 2.3$ ) can guarantee an efficiency of at least 10 dB.

## 7 REFERENCES

- [1] D. Thompson. Railway noise and vibration, mechanisms, modelling and means of control, 2010 Elsevier Ltd.
- [2] S. François, L. Pyl, H. Masoumi, G. Degrande. The influence of dynamic soil-structure interaction on traffic induced vibrations in buildings. *Soil Dynamics and Earthquake Engineering*, 27 (7), 655-674, 2007.
- [3] A. T. Peplow and A. M. Kaynia. Prediction and validation of traffic vibration reduction due to cement column stabilization. *Soil Dynamics and Earthquake Engineering*, 27:793–802, 2007.
- [4] L. Pyl, G. Degrande, G. Lombaert, W. Haegeman. Validation of a source-receiver model for road traffic-induced vibrations in buildings. I: Source model. *Journal of engineering mechanics-asce*, 130 (12), 1377-1393, 2004.
- [5] K.R. Massarsch. Mitigation of traffic-induced ground vibration. In *Proceedings of the 11th International Conference on Soil Dynamics and Earthquake Engineering*, Berkeley, California, USA, June 2004.
- [6] X. Sheng, C.J.C. Jones, and D.J. Thompson. Responses of infinite periodic structures to moving or stationary harmonic loads. *Journal of Sound and Vibration*, 282:125–149, 2005.
- [7] S. François, M. Schevenels, P. Galvin, G. Lombaert, and G. Degrande. A 2.5D coupled FE-BE methodology for the dynamic interaction between longitudinally invariant structures and a layered half space. *Computer methods in applied mechanics and engineering*, 199(23-24):1536 – 1548, 2010.
- [8] M. Schevenels, S. François, and G. Degrande. EDT: An ElastoDynamics Toolbox for MATLAB. *Computers & Geosciences*, 35(8):1752–1754, 2009.
- [9] K. Itoh, X. Zeng, O. Murata, and O. Kusakabe. Centrifugal simulation on vibration reduction generated by high-speed trains using rubber-modified asphalt foundation and EPS barrier. *International Journal of Physical Modelling in geotechnics*, 2:1–10, 2003.
- [10] J. Garnier, C. Gaudin, S.M. Springman, P.J. Culligan, D. Goodings, D. König, B. Kutter, R. Phillips, M.F. Randolph, and L. Thorel. Catalogue of scaling laws and similitude questions in geotechnical centrifuge modelling. *International Journal of Physical Modelling in geotechnics*, 7(3):1–24, 2007.